Journal of Materials Chemistry A

Optimization of Active Layer Morphology by Small Molecule Donor Design Enables over 15% Efficiency in All-Small-Molecule Solar Cells

Journal:	*Journal of Materials Chemistry A*
Manuscript ID	TA-ART-12-2020-012242.R2
Article Type:	Paper
Date Submitted by the Author:	20-Apr-2021

Complete List of Authors:	An, Cunbin; Institute of Chemistry Chinese Academy of Sciences, Qin, Yunpeng; North Carolina State University, Physics Zhang, Tao; Institute of Chemistry Chinese Academy of Sciences Lv, Qianglong; Institute of Chemistry Chinese Academy of Sciences Qin, Jinzhao ; Institute of Chemistry Chinese Academy of Sciences Zhang, Shaoqing; University of Science and Technology Beijing, School of Chemistry and Biological Engineering He, Chang; Institute of Chemistry, Chinese Academy of Sciences, Ade, Harald; North Carolina State University, Physics Hou, Jianhui ; Institute of Chemistry, Chinese Academy of Sciences,

ARTICLE

Optimization of Active Layer Morphology by Small Molecule Donor Design Enables over 15% Efficiency in Small-Molecule Organic Solar Cells

Received 00th January 20xx,
Accepted 00th January 20xx

DOI: 10.1039/x0xx00000x

Cunbin An,[a] Yunpeng Qin,[c] Tao Zhang,[a] Qianglong Lv,[a] Jinzhao Qin,[ab] Shaoqing Zhang,[a] Chang He,[a] Harald Ade,[c] Jianhui Hou*[ab]

Molecular innovation is highly important to achieve high-efficient small-molecule organic solar cells (SMOSCs). Herein, we report two small molecule donors, **B3T-T** and **B3T-P**, differing only in conjugated side chains with thienyl group in the former and phenyl unit in the latter. Surprisingly, both small molecule donors show distinct electron density distribution and electrostatic potential along the conjugated backbone. **B3T-P** has a much higher dipole moment (0.920 D) than **B3T-T** (0.237 D). In SMOSCs, the **B3T-T**: BO-4Cl-based device shows a decent power conversion efficiency (PCE) of 11.1%. In contrast, the **B3T-P**: BO-4Cl-based device gives an outstanding PCE of 15.2%, which is one of the highest values among SMOSCs. Compared to the **B3T-P**-based device, although the **B3T-T**-based device has a large enough driving force for exciton separation and an extremely low non-radiative recombination voltage loss (0.168 V) for achieving high open-circuit voltage, the large domain size (63 nm) and low domain purity in the **B3T-T**: BO-4Cl-based device leads its relatively low short-circuit current density and fill factor, thus giving a low PCE. This result may pave the way to rational design SM donors for highly efficient SMOSCs.

Introduction

Bulk heterojunction (BHJ) organic solar cell (OSC) is a promising technology for harvesting clean solar energy due to its advantages of light-weight, flexible, large-area photovoltaic devices via solution processing or semi-transparency.[1-4] In BHJ OSCs, active layer material, included an electron donor and an electron acceptor, plays a vital role in improving power conversion efficiency (PCE). Based on the attributes of active layer material, OSCs can be divide into polymer solar cells (PSCs), all-polymer solar cells (all-PSCs), and small-molecule OSCs (SMOSCs). Compared to other types of OSCs, ASM-OSCs show great potential in commercialization and the achievement of excellent PCE due to several advantages in small molecules over conjugated polymers, such as well-defined chemical structures, reproducible synthesis, relative ease of purification, and low energetic disorder.[5-11] However, the PCEs of SMOSCs lag far behind PSCs that have reached 18%.[12-18] Currently, the best ternary SMOSCs has achieved a PCE of 15.9%,[18] which was fabricated by one donor material of ZnP-TBO and two acceptors of 6TIC and 4TIC. One of the critical reason is that understanding the relationship between molecular structure and device performance is lagging due to the insufficiency of high-performance SM donors compared to polymer donors. Hence, it is highly desired to develop novel SM donors for high-performance SMOSCs.

Compared to the state-of-the-art non-fullerene (NF)-based PSCs, the inferior PCEs of NF-based SMOSCs are usually caused by low short-circuit current density (J_{SC}) and fill factor (FF),[19, 20] which are mainly attributed to the unfavourable BHJ morphology, resulting in inefficient exciton dissociation, low charge transportation, and serious charge recombination. A favourable BHJ morphology in OSC is the formation of nanoscale bi-continuous phase separation with high domain purity and proper domain sizes. For PSCs, a polymer donor with pre-aggregation in solution can form an interpenetrating network in film by spin-coating method.[21, 22] This advantage makes it easier to obtain favourable BHJ morphology with an NF acceptor. Currently, some strategies have been developed to optimize BHJ morphology by tuning polymer donor's aggregation in PSCs.[23, 24] For SMOSCs, however, SM donor cannot form efficient pre-aggregation property in solution due to the lack of strong enough intermolecular entanglement and intermolecular interaction on such a short molecular skeleton. Meanwhile, the SM donor has a closer chemical structure and molecular size with NF acceptor compared to polymer donor. Therefore, it is more challenging to achieve favourable BHJ morphology by material design and optimization in SMOSCs.

BHJ morphologies of SMOSCs have been proved to be optimized properly by some external factors, such as solvent additive, solvent vapor annealing (SVA), and thermal annealing (TA), and so on.[25-27] Based on these optimization methods, however, it is hard to achieve the best J_{SC} and FF simultaneously due to the limitation of SM donors' inherent property. The breakthrough in PCE of SMOSCs is highly dependent on the development of new active materials. This is because the active layer morphology is mainly contributed by the

[a] Beijing National Laboratory for Molecular Sciences, State Key Laboratory of Polymer Physics and Chemistry, Institute of Chemistry, Chinese Academy of Sciences, Beijing 100190, China. E-mail: hjhzlz@iccas.ac.cn; Tel.: +86-10-82615900.
[b] University of Chinese Academy of Sciences, Beijing 100049, China.
[c] Department of Physics and Organic and Carbon Electronics Laboratories (ORaCEL), North Carolina State University, Raleigh, NC 27695, USA
† Footnotes relating to the title and/or authors should appear here.
Electronic Supplementary Information (ESI) available: [details of any supplementary information available should be included here]. See DOI: 10.1039/x0xx00000x

intermolecular interactions of active layer materials. Recently, the researchers have found that the enhanced the crystallinity of small molecule donor can improve BHJ morphology and obtain high-efficiency binary SMOSCs. For example, Lu, et al. used Cl atoms to replace a pair of alkyl chain of BTR to obtain a donor material, BTR-Cl, which has a higher crystallinity compared to the BTR. Such property made BTR-Cl form a better phase-separation with electron acceptor of Y6. Thus, the BTR-Cl:Y6-based device produced a PCE of 13.6%.[17] Wei et al. designed a highly crystalline small molecule donor, ZR1, by fusing two thiophenes onto the central unit, which yielded hierarchical morphology with Y6 and achieved a PCE of 14.3%.[10] Recently, our group also synthesized a highly crystalline small molecule donor, B1, which showed a smaller π-π distance than that of referenced BTR. After blending with an electron acceptor of BO-4Cl (Fig. 1d), B1 exhibited stronger interactions with BO-4Cl compared to the BTR and BO-4Cl, leading to a better BHJ morphology. B1-based device showed a best PCE of 15.3% among binary SMOSCs to date.[15] Considering that the electron acceptor of the Y6 series show excellent device performances in OSCs, it is highly desired to develop novel SM donors to match this kind of acceptors and understand their relationship between molecular structures, BHJ morphologies and photovoltaic efficiencies.

To further understand the influence pf phenyl as conjugated side chains in small molecules on the photovoltaic performances, herein, we reported two SM donors (**B3T-T** and **B3T-P**, Scheme 1), which have different conjugated side chains of thienyl unit in the former and phenyl group in the latter. We deeply considered the following two points to achieve rational molecular design. Firstly, the thienyl unit as a conjugated side will produce few disordered molecular geometries in a given target molecule due to its non-axisymmetric structure. Therefore, the *meta*-position substituted benzene was used as a conjugated side chain to keep similar molecular geometries. Secondly, the *meta*-position substituted benzene as conjugated side chain could downshift high occupied molecular orbital (HOMO) levels or reduce non-radiative recombination energy loss by enhancing device electroluminescence quantum efficiency in a given molecule, thus outputting a relatively high open-circuit voltage (V_{OC}) in an OSC.[28, 29] Thus, the fluorine atoms were introduced onto pendent thiophene units to maintain an approximate initial V_{OC} in both SM donor-based OSCs. When both small donors were blended with the NF acceptor of BO-4Cl, the **B3T-T**: BO-4Cl-based device only gave a PCE of 11.1%, while **B3T-P**: BO-4Cl-based device showed an impressive PCE of 15.2%. Such different PCEs for both SM donors were carefully analysed by investigating their inherent properties, BHJ morphology, and energy losses in both devices.

Results and discussion

Synthesis and Characterizations

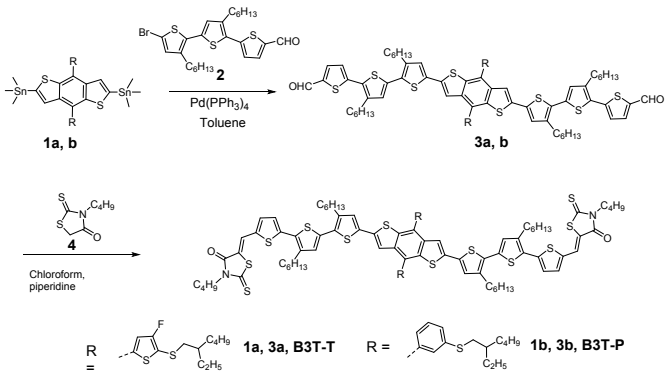

Scheme 1. Synthetic routes for the **B3T-T** and **B3T-P**.

Both SM donors were synthesized using two-step reactions from reported precursors as shown in **Scheme 1**.[28, 30, 31] Dialdehyde compound **3a** (**3b**) was synthesized by Stille coupling reaction between corresponding distannyl compound **1a** (**1b**) and compound **2** in a high yield of 91% (90%). Subsequently, the dialdehyde compound **3a** (**3b**) was transformed into desired SM donor of **B3T-T** (**B3T-P**) by Knoevenagel reactions with 3-butyl-2-thioxothiazolidin-4-one (**4**) in a good yield of 85% (83%). The detailed synthetic procedures were described in the Supporting Information. Both SM donors have good solubility in tetrahydrofuran and chloroform, which is beneficial for the fabrication of photovoltaic devices by solution processing. The thermogravimetric analysis shows that **B3T-P** has a decomposition temperature with 5% weight loss up to 394 °C, which is more thermal stability than **B3T-T** (372 °C, Fig. S1, ESI†). Besides, the differential scanning calorimetry (DSC) measurements reveal that both SM donors show clear melting points (T_m) of 273 and 222 °C on the heating and recrystallization point (T_c) of 217 and 193 °C on the cooling for **B3T-T** and **B3T-P**, respectively (Fig. 1a). The lower T_m and T_c of **B3T-P** indicates that the phenyl group as conjugated side chains could reduce the molecular thermal robustness compared to that of thienyl as conjugated side chains.[32]

Optical and electrochemical properties

As shown in Fig. 1b, both SM donors show similar absorption profiles with a maximum absorption wavelength (λ_{max}) at 518 nm in dilute chloroform solution at room temperature. The corresponding molar extinction coefficients are 1.0×10^5 and 1.1×10^5 M^{-1} cm^{-1} for **B3T-T** and **B3T-P**, respectively (Fig. S2a, ESI†). Compared to their absorption spectra in solution, both SM donors exhibit the same red-shift of the λ_{max} to 576 nm in films but the difference is that **B3T-T** has a stronger and more bathochromic shoulder peak at 629 nm than that of **B3T-P** (621 nm), which suggests that **B3T-P** has a weaker intermolecular interaction or aggregation ability than those of **B3T-T** in solid-state. It is consistent with the observation from DSC measurements. The optical bandgap (E_g^{opt}) of **B3T-T** and **B3T-P** are 1.80 and 1.81 eV, respectively, estimated by their absorption onset of the films. Such E_g^{opt}s of both SM donors exhibit the well complementary absorption spectra with the NF acceptor of BO-4Cl, which are expected to achieve high J_{SC}s in resulting photovoltaic devices.

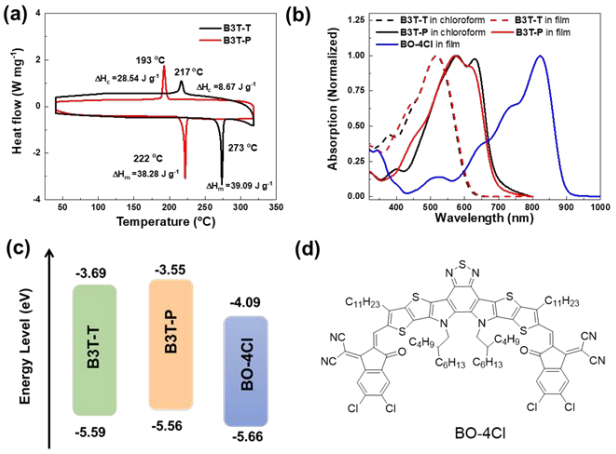

Fig. 1. (a) DSC curves of **B3T-T** and **B3T-P** at a heating and cooling rate of 10 ºC min^{-1} under nitrogen; The absorption spectra (b) and energy level diagram (c) of **B3T-T**, **B3T-P**, and BO-4Cl; (d) Chemical structure of BO-4Cl.

The HOMOs of both SM donors are evaluated by cyclic voltammetry (CV). Their oxidation and reduction curves are shown in Fig. S3 (ESI†). Based on the onsets of first oxidation peaks and the equation of $E_{HOMO} = -(E_{Ox} - E^{1/2}_{Fc/Fc+} + 4.8)\ eV$, the HOMO values were estimated to be -5.59 eV for **B3T-T** and -5.56 eV for **B3T-P**, respectively. The corresponding lowest unoccupied molecular orbitals (LUMO) of both SM donors were calculated to be -3.69 and -3.65 eV, based on the equation $E_{LUMO} = E_{HOMO} + E_g^{opt}$.[33] It should be noted that these E_{LUMO} should be larger than those of the values obtained from CV measurements due to the inclusion of exciton binding energy in this equation.[34] The energy level alignments of photoactive materials are illustrated in Fig. 1c. The HOMO energy offset in **B3T-T**: BO-4Cl is 0.07 eV, which is large enough to achieve efficient exciton dissociation in NF-based OSCs.

Density functional theory calculations

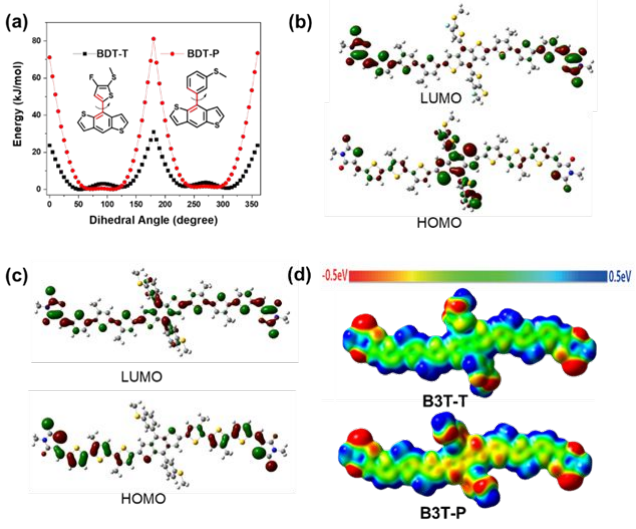

Fig. 2 (a)The total energy scans dependent on dihedral angels for model compounds BDT-T and BDT-P. Electron density distributions onto LUMO and HOMO for **B3T-T** (b) and **B3T-P** (c); (d) ESP distributions of both SM donors.

The torsional barrier energies of both conjugated side chains were investigated by employing density functional theory (DFT) calculation with the base set of B3LYP/6-31 (d, p). Considering the same conjugated main chains of both SM donors, the model compounds of BDT-T and BDT-P were carried out to replace **B3T-T** and **B3T-P** as shown in Fig. 2a. The significantly big torsional barrier energy in BDT-P implies that the **B3T-P** has a more stable conformation than **B3T-T**. To further understand the inherent property of SM donors, the electron density distribution, molecular electrostatic potential (ESP) distribution and dipole moments were also calculated by DFT calculations using the above-mentioned base set.[35] As shown in Fig. 2b-d, **B3T-T** shows a typical electron density distribution that electron density locates electron-withdrawing and electron-donating units for LUMO and HOMO, respectively. Surprisingly, **B3T-P** presents a significantly different phenomenon that the electron density distributes onto the whole conjugated backbone for LUMO and both outsides of **B3T-P** for HOMO. The ESP image also confirms different electrostatic potential distribution onto the centres of both SM donors. Additionally, **B3T-P** has a dipole moment up to 0.920 D, which is much higher than **B3T-T** (0.237 D). A higher dipole moment facilitates enhanced ordering between the donor and the acceptor in OSCs, which improves the charge mobility between the donor-acceptor.[36] Overall, such different electronic features in both SM donors should affect their organization in blend films, resulting in the different BHJ morphologies and photovoltaic performances in SMOSCs.

Photovoltaic performance, charge transport properties and recombination mechanisms

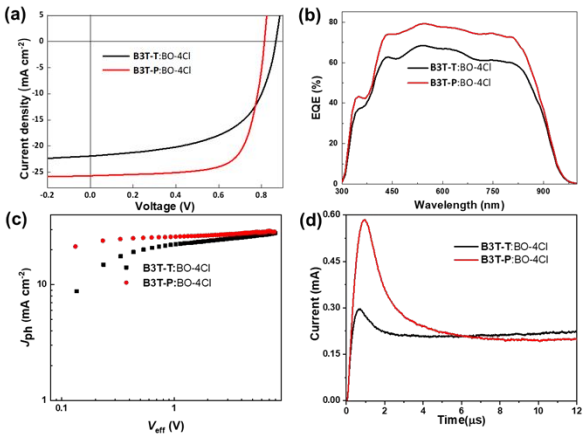

Fig. 3 (a) The *J*–*V* (a) and EQE (b) curves of the **B3T-T**: BO-4Cl- and **B3T-P**: BO-4Cl-based SMOSCs. (c) The J_{ph} plotted against the V_{eff} for the optimal **B3T-T**- and **B3T-P**-based SMOSCs. (d) The photo-CELIV transients of **B3T-T**- and **B3T-P**-based SMOSCs.

To investigate the photovoltaic performances of both SM donors with BO-4Cl, we employed a conventional device structure of indium tin oxide (ITO)/poly(3,4-ethylene dioxythiophene): poly(styrene sulfonate)(PEDOT: PSS)/SM donor: BO-4Cl/PFN-Br/Al. The BHJ morphology of the active layer was carefully optimized by

changing the SVA time, donor/acceptor weight ratios (w/w) and the thickness of active layer. The detailed data are summarized in Table S1-S6 (ESI†). The current density-voltage (*J*-*V*) curves of the optimal OSCs are displayed in Fig. 3a, and the corresponding photovoltaic parameters are collected in Table 1. Without any treatment, the **B3T-T**: BO-4Cl-based device exhibited a PCE of 0.9%, with a V_{OC} of 0.925 V, a J_{SC} of 3.2 mA cm^{-2}, and an FF of 0.300, the **B3T-P**: BO-4Cl-based device showed a PCE of 1.0%, with a V_{OC} of 0.899 V, a J_{SC} of 3.5 mA cm^{-2}, and an FF of 0.305. The different V_{OC}s of both devices could be attributed to their HOMO levels. When both devices were treated by SVA using chlorobenzene for 55 seconds, the **B3T-T**: BO-4Cl-based device gave a PCE of 11.1% with a V_{OC} of 0.867 V, a J_{SC} of 21.9 mA cm^{-2}, and an FF of 0.582. In contrast, the **B3T-P**: BO-4Cl-based device showed an outstanding PCE of 15.2%, with a V_{OC} of 0.815 V, and significant improvement J_{SC} of 25.7 mA cm^{-2} and FF of 0.724. To the best of our knowledge, it is one of the highest PCE values among SMOSCs. Fig. 3b presents the external quantum efficiency (EQE) curves of both optimized SMOSCs. Although both devices had the same photo response region from 300 to1000 nm, **B3T-P**-based SM-OSC exhibited a higher EQE response in the whole region than that of **B3T-T**-based SMOSC. The J_{SC} values were calculated from the integration of the EQE data to be 20.9 and 24.5 mA cm^{-2} for **B3T-T**- and **B3T-P**-based SMOSCs, respectively. These values are close to the J_{SC} values obtained from the *J*–*V* measurements below 5% mismatch. The molar extinction coefficients of blend films at the absorption peak of 576 nm are calculated to be 6.1×10^4 and 6.2×10^4 cm^{-1} for **B3T-T**:BO-4Cl and **B3T-P**:BO-4Cl, respectively (Fig. S2b, ESI†). Such minor difference in molar extinction coefficients of both blend films have a weak influence on their corresponding SMOSCs, thus the significantly different J_{SC}s in both devices should be major attributed to their different BHJ morphology.

Table 1. Detailed photovoltaic parameters of the **B3T-T**: BO-4Cl- and **B3T-P**: BO-4Cl-based SMOSCs under simulated AM 1.5G (100 mW cm^{-2}) illumination.[a]

Materials	V_{OC} (V)	J_{SC} (mA cm^{-2})	FF	PCE (%)
B3T-T:BO-4Cl	0.865±0.004 (0.867)	21.8±0.44 （21.9）	0.583±0.02 （58.21）	11.0±0.41 （11.1）
B3T-P:BO-4Cl	0.813±0.003 （0.815）	25.6±0.31 （25.7）	0.717±0.02 （0.724）	14.9±0.17 （15.2）

[a]Average PCE values were obtained from 10 devices. The parameters based on the best device are shown in parentheses

To understand the effect of the conjugated side chains in both SM donors on exciton dissociation and charge collection in SMOSCs, the measurement of photogenerated current density (J_{ph}) against effective voltage (V_{eff}) was carried out.[37] The J_{ph} is the difference between light current density (J_L) and dark current density (J_D), the V_{eff} is defined as the difference value between the compensation voltage (V_0, determined when the J_{ph} is zero) and the applied external voltage bias (V_{bias}). The exciton dissociation probability (P_{diss}) is estimated by the equation of $P_{diss} = J_{ph}/J_{sat}$, where J_{sat} is the saturation photocurrent density. As shown in Fig. 3c, the P_{diss} of **B3T-T**: BO-4Cl- and **B3T-P**: BO-4Cl-based devices were calculated to be 84% and 91%, respectively, under short circuit conditions, indicating that the **B3T-P**: BO-4Cl-based device has a higher efficiency in the photogenerated exciton dissociation and charge collection.

To investigate the effect of the conjugated side chain in both SM donors on charge transport properties of the SMOSCs, we firstly employed photo-induced charge-carrier extraction in linearly increasing voltage (photo-CELIV) to estimate their charge carrier mobilities in both devices.[38] The mobilities of both devices were obtain from five optimal devices, the representative curves were shown in Fig. 3d, the **B3T-T**-based device gives a mobility of $2.6 \pm 0.13 \times 10^{-4}$ cm^2 V^{-1} s^{-1}, while the **B3T-P**-based device exhibits a higher mobility of $4.3 \pm 0.17 \times 10^{-4}$ cm^2 V^{-1} s^{-1}. To further understand the charge hole and electron charge transport abilities in films, space-charge limited current (SCLC) measurements were also performed on the neat SM donors and blend films.[39] The corresponding films were treated according to the conditions of the optimal devices. The mobilities of these films were obtain from five-time measurements, the representative curves were shown in Fig. S4 and S5 (ESI†), the hole mobility (μ_h) of the neat **B3T-T** film is $2.37 \pm 0.14 \times 10^{-4}$ cm^2 V^{-1} s^{-1}, which is slightly higher than that of the neat **B3T-P** film ($2.25 \pm 0.08 \times 10^{-4}$ cm^2 V^{-1} s^{-1}), which could be attributed to the stronger intermolecular interactions and ordering arrangement in **B3T-T** film. After blending with BO-4Cl, the μ_h of **B3T-T**: BO-4Cl blend film is significantly reduced to $5.0 \pm 0.07 \times 10^{-5}$ cm^2 V^{-1} s^{-1}, while the μ_h of **B3T-P**: BO-4Cl blend film is slightly decreased to $1.0 \pm 0.03 \times 10^{-4}$ cm^2 V^{-1} s^{-1}. Additionally, the electron mobilities (μ_es) of both blend films are $1.8 \pm 0.07 \times 10^{-4}$ and $1.1 \pm 0.03 \times 10^{-4}$ cm^2 V^{-1} s^{-1} for **B3T-T**: BO-4Cl and **B3T-P**: BO-4Cl films, respectively. **B3T-P**: BO-4Cl film gives a more balanced charge carrier mobilities (μ_e/μ_h = 1.1) than that of **B3T-T**: BO-4Cl film (μ_e/μ_h = 3.6), which is consistent with the higher FF in **B3T-P**-based SMOSCs.

To clarify the different J_{SC} and FF values in both SMOSCs, the charge recombination mechanism was further studied by measuring *J*-*V* curves as a function of illumination intensity (P_{light}).[40, 41] The relationship between V_{OC} and P_{light} was measured, as shown in Fig. S6a (ESI†). The **B3T-T**- and **B3T-P**-based SMOSCs show slopes of 1.21 KT/q and 1.11 KT/q, respectively. The smaller slope for the **B3T-P**-based SMOSC suggests the suppressed Shockley-Read-Hall recombination under the open-circuit condition. The relationship between J_{SC} and P_{light} was also investigated, which was described as a power-law equation of $J_{SC} \propto P_{light}^{S}$, when the S value is approaching 1, the photovoltaic device has negligible bimolecular recombination.[40, 41] As shown in Fig. S6b (ESI†), the S values of both SMOSCs were calculated to be 0.94 and 0.99 for **B3T-T**- and **B3T-P**-based devices, respectively, which indicates that **B3T-P**-based SM-OSC has weaker bimolecular recombination than that of **B3T-T**-based device. Overall, this result agrees well with their photovoltaic performances.

Energy losses

Table 2. Detailed V_{OC} losses of optimal **B3T-T**- and **B3T-P**-based SMOSCs.

Active layer	E_g (eV)	V_{OC} (V)	E_{loss} (eV)	E_{CT} (eV)	ΔE_{CT} (eV)	$\Delta V_{non\text{-}rad}$ (V)	EQE_{EL}
B3T-T:BO-4Cl	1.397	0.867	0.530	1.342	0.055	0.186	7.50×10^{-4}
B3T-P:BO-4Cl	1.391	0.815	0.576	1.342	0.049	0.234	1.17×10^{-4}

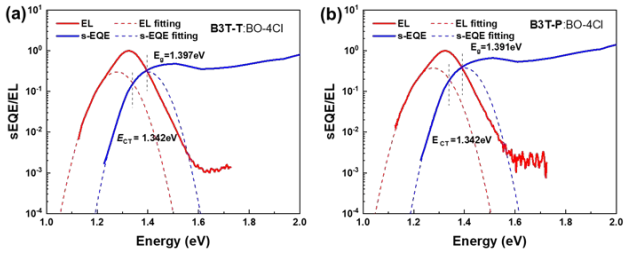

Fig. 4 (a) Reduced EQE and EL spectra of (a) **B3T-T**- and (b) **B3T-P**-based devices.

To understand the difference in V_{OC}s of both devices, their energy losses (E_{loss}) were investigated in detail. The E_{loss} of the photovoltaic cell can be divided into three parts as the equation of $E_{loss} = E_g - q\Delta V_{OC} = q\Delta V_{rad} + \Delta E_{CT} + q\Delta V_{non-rad}$ (1).[42] Where bandgap (E_g) of these devices were calculated from the intersection of the electroluminescence and EQE curve of the blend film; q is element charge; ΔV_{rad} is the voltage loss due to radiative recombination, which is inevitable in all type of solar cells; $\Delta E_{CT} = E_g - E_{CT}$, where E_{CT} is the charge state of blend film, which provide driving force for the exciton separation. $\Delta V_{non\text{-}rad}$ is the voltage loss due to non-radiative recombination, which can be calculated from the equation of $qV_{OC}^{non-rad} = -kT\ln(EQE_{EL})$, where k is the Boltzmann constant, T is absolute temperature, and EQE_{EL} is electroluminescence quantum efficiency of the solar cell when charge carriers are injected into the device under dark condition.[43] The detailed energy losses are collected in Table 2. As shown in Fig. 4, the E_gs of both devices were calculated to 1.397 and 1.391 eV for **B3T-T**: BO-4Cl and **B3T-P**: BO-4Cl films, respectively. The total E_{loss}s of both devices were 0.530 and 0.576 eV according to the equation (1) for **B3T-T**- and **B3T-P**-based SMOSCs, respectively. The E_{CT}s of both blend films were calculated according to the reported method.[44, 45] Both blend films have the same E_{CT} of 1.342 eV as shown in Fig. 4, thus their corresponding ΔE_{CT} are 0.055 and 0.049 eV for **B3T-T**- and **B3T-P**-based SMOSCs, respectively. For the $q\Delta V_{non\text{-}rad}$, **B3T-T**-based device showed a much higher EQE_{EL} of 7.50×10^{-4} than that of **B3T- P**-based device (1.17×10^{-4}), thus producing to a much smaller $q\Delta V_{non\text{-}rad}$ of 0.186 eV for the former and bigger $q\Delta V_{non\text{-}rad}$ of 0.234 eV for the latter. Based on these results, we found the **B3T-T**-based device has a bigger driving force for the exciton separation than that in **B3T-P**-based device due to its larger ΔE_{CT}. Therefore, the significantly low J_{SC} and FF in **B3T-T**-based should be attributed to the inferior BHJ morphology. This result can be further supported that phenyl as side chains in small-molecule donor is beneficial for optimizing BHJ morphology. Additionally, the **B3T-T**-based the device has a small non-radiative loss, which reached the same level compared to PSCs.[46, 47] According to the previous prediction, a photovoltaic cell with $q\Delta V_{non\text{-}rad}$ of 0.19 eV and EQE photoresponse edge could achieve more than 18% efficiency, if the BHJ morphology issue is overcome.[43]

BHJ morphologies and organization

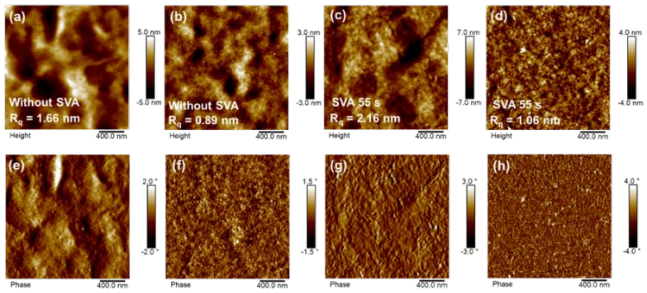

Fig. 5 AFM height images of (a) **B3T-T**:BO-4Cl, (b) **B3T-P**:BO-4Cl, (c) **B3T-T**:BO-4Cl and (d) **B3T-P**:BO-4Cl films. Phase images of (e) **B3T-T**:BO-4Cl, (f) **B3T-P**:BO-4Cl, (g) **B3T-T**:BO-4Cl and (h) **B3T-P**:BO-4Cl films.

To further understand the effect of the conjugated side chain in both SM donors on device performances, the surface morphologies of the blend films were investigated by atomic force microscopy (AFM) as shown in **Fig. 5**. Without SVA treatment, the heigh images show that **B3T-P**:BO-4Cl film exhibits a smoother surface with a mean-square surface roughness (Rq) of 0.89 than that of **B3T-T**:BO-4Cl film (1.66 nm), which could be attributed to the weaker crystallinity of **B3T-P**. The phase images show that **B3T-T**:BO-4Cl shows obvious large-scale phase separation, and the **B3T-P**:BO-4Cl shows interpenetrating network but without clear phase separation, which are directly related to their low J_{SC}s and *FF*s. After these blends were treated by SVA for 55 s using chlorobenzene, the surface roughness of both blend films is slightly increased due to the re-organization of small molecules. The phase images show that the scale of phase separation in **B3T-T**:BO-4Cl film was obviously improved compared to the initial film, but is still larger than that of **B3T-P**:BO-4Cl film, more importantly, the nanofiber-like structure can be observed in **B3T-P**:BO-4Cl film, which is of vital importance for B3T-P-based SM-OSC to achieve a higher PCE.

To deeply understand the difference of photovoltaic performance caused by the changed conjugated side chains, grazing incidence wide-angle X-ray scattering (GIWAXS) measurements were carried out to determine the molecular structural organizations of both neat SM donors and their blend films.[48] The GIWAXS patterns of the neat donor and blend films are presented in **Fig. 6**. The corresponding data are collected in Table S7 (ESI†). The neat films of both SM donors exhibit strong π-π (010) diffraction peaks in in-plane (IP) direction and lamella stacking (100), (200), (300) peaks in out-of-plane (OOP) direction. This indicates that both SM donors have the edge-on organization and are highly ordered. Although **B3T-P** has the same π stacking distance of (0.36 nm) with **B3T-T**, the coherence

length (CL) of π-π stacking in **B3T-P** (6.47 nm) is smaller than that of **B3T-T** (6.68 nm). Meanwhile, **B3T-P** also shows a larger lamella stacking distance of 18.36 nm than that of **B3T-T** (17.99 nm). These results further confirm that **B3T-P** has a weaker molecular packing and intermolecular interaction compared to **B3T-T**. It also can explain that **B3T-P** has slightly lower hole mobility than that of **B3T-T**. After blending with BO-4Cl, both blend films exhibit face-on arrangement, which is beneficial for charge transport in OSCs towards the electrodes. Simultaneously, the (200) and (300) diffraction peaks in blend films disappear compared to the neat SM donor films, indicating that both SM donors' molecular packing was suppressed by introducing the BO-4Cl. Importantly, **B3T-P**: BO-4Cl film shows a smaller π-π distance of 0.34 nm and longer CL of 5.66 nm than those of **B3T-T**: BO-4Cl film (0.35 nm and 3.88 nm), which is consistent with their corresponding device performances. To elucidate the observed J_{SC} and FF changes in both SMOSCs, the domain size and purity of both blend films were also investigated by resonant soft X-ray scattering (RSoXS) at a photon energy of 284.2 eV, as shown in Fig. 6f.[49-51] The RSoXS data reveal that the average domain sizes are 63 and 19 nm for the films of **B3T-T**: BO-4Cl and **B3T-P**: BO-4Cl, respectively. The large domain sizes of **B3T-T**: BO-4Cl is harmful for exciton dissociation and charge transport. In contrast, the domain sizes of **B3T-P**: BO-4Cl is close to the ideal value of 20-30 nm for highly efficient exciton dissociation in OSCs.[22] Additionally, the relative composition variation, which relates monotonically to the domain purity, of **B3T-T**: BO-4Cl is 0.87, which is lower than **B3T-P**: BO-4Cl film. This result implies that **B3T-T**: BO-4Cl film has a strong intermixing phase, thus suffering from serious charge recombination, which is in good agreement with the light intensity dependent V_{OC} and J_{SC} measurements. Overall, these experiments support the superior J_{SC}, FF, and PCE of the **B3T-P**: BO-4Cl-based device compared to those of the **B3T-T**: BO-4Cl-based device.

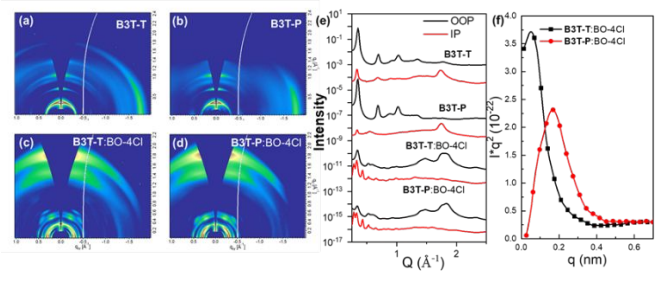

Fig. 6 GIWAXS 2D patterns of (a) **B3T-T**, (b) **B3T-P**, (c) **B3T-T**:BO-4Cl and (d) **B3T-P**:BO-4Cl. (e) The 1D GIWAXS profiles of pure and blend films. (f) Lorentz-corrected RSoXS profiles for blend films.

Conclusions

In summary, we designed and synthesized two SM donors of **B3T-T** and **B3T-P,** which only differ in the conjugated side chains. Both SM donors have a similar chemical structure and optical property, but they show significantly different molecular packing and electronic properties, such as electron density and ESP distribution onto the conjugated backbone as well as dipole moment. In the SMOSCs, the **B3T-T**-based device only yielded a PCE of 11.1%, a V_{OC} of 0.867 V, a J_{SC} of 21.9 mA cm^{-2}, and an FF of 0.582. In contrast, the **B3T-P**-based device gave an outstanding PCE of 15.2%, with a V_{OC} of 0.815 V, and significant improvement J_{SC} of 25.7 mA cm^{-2} and FF of 0.724, which is one of the highest PCE among SMOSCs. The offset (ΔV_{OC} = 0.052 V) in V_{OC} of both devices is primarily attributed to their difference in $\Delta V_{non\text{-}rad}$ (0.048 V). Compared to **B3T-T**, the different electron feature in **B3T-P** may maintain more efficient intermolecular interaction between **B3T-P** and BO-4Cl, which is beneficial to form favourable phase separation with balanced charge carrier mobilities, longer CL, proper domain size, and high domain purity. These results should be the main reasons that the **B3T-P**-based device has a higher PCE with an improved J_{SC} and FF. Overall, our results show that using of phenyl conjugated side chain in SM donors is an important tool to optimize BHJ morphologies and achieve highly efficient SMOSCs.

Conflicts of interest

There are no conflicts to declare.

Acknowledgements

The authors acknowledge the financial support from the National Natural Science Foundation of China (Grant No. 21734008, 51673201, 21835006, 51873217), Beijing National Laboratory for Molecular Sciences (BNLMS-CXXM-201903). Y. Q. and H. A. are supported by ONR grant N000142012155. X-ray data were acquired at beamline 7.3.3 and 11.0.1.2 at the Advanced Light Source, which is supported by the Director, Office of Science, Office of Basic Energy Sciences, of the U.S. Department of Energy under Contract No. DE-AC02-05CH11231

Notes and references

1. G. Yu, J. Gao, J. C. Hummelen, F. Wudl and A. J. Heeger, *Science*, 1995, **270**, 1789.
2. C. Liu, K. Wang, X. Gong and A. J. Heeger, *Chem. Soc. Rev.*, 2016, **45**, 4825.
3. Y. Li, *Acc. Chem. Res.*, 2012, **45**, 723.
4. E. Ravishankar, R. E. Booth, C. Saravitz, H. Sederoff, H. W. Ade and B. T. O'Connor, *Joule*, 2020, **4**, 490.
5. C. He and J. Hou, *Acta Phys. -Chim. Sin.*, 2018, **34**, 1202.
6. S. D. Collins, N. A. Ran, M. C. Heiber and T.-Q. Nguyen, *Adv. Energy Mater.*, 2017, **7**, 1602242.
7. B. Walker, C. Kim and T.-Q. Nguyen, *Chem. Mater.*, 2011, **23**, 470.
8. M. Li, K. Gao, X. Wan, Q. Zhang, B. Kan, R. Xia, F. Liu, X. Yang, H. Feng, W. Ni, Y. Wang, J. Peng, H. Zhang, Z. Liang, H.-L. Yip, X. Peng, Y. Cao and Y. Chen, *Nat. Photon.*, 2017, **11**, 85.
9. M. Li, F. Liu, X. Wan, W. Ni, B. Kan, H. Feng, Q. Zhang, X. Yang, Y. Wang, Y. Zhang, Y. Shen, T. P. Russell and Y. Chen, *Adv. Mater.*, 2015, **27**, 6296.
10. R. Zhou, Z. Jiang, C. Yang, J. Yu, J. Feng, M. A. Adil, D. Deng, W. Zou, J. Zhang, K. Lu, W. Ma, F. Gao and Z. Wei, *Nat. Commun.*, 2019, **10**, 5393.
11. J. Ge, L. Xie, R. Peng, B. Fanady, J. Huang, W. Song, T. Yan, W. Zhang and Z. Ge, *Angew. Chem. Int. Ed.*, 2020, **59**, 2808.

12. Q. Liu, Y. Jiang, K. Jin, J. Qin, J. Xu, W. Li, J. Xiong, J. Liu, Z. Xiao, K. Sun, S. Yang, X. Zhang and L. Ding, *Sci. Bull.*, 2020, **65**, 272.
13. Y. Lin, Y. Firdaus, F. H. Isikgor, M. I. Nugraha, E. Yengel, G. T. Harrison, R. Hallani, A. El Labban, H. Faber, C. Ma, X. Zheng, A. S. Subbiah, C. T. Howells, O. M. Bakr, I. McCulloch, S. De Wolf, L. Tsetseris and T. D. Anthopoulos, *ACS Energy Lett.*, 2020, **5**, 2935.
14. Y. Cui, H. Yao, J. Zhang, K. Xian, T. Zhang, L. Hong, Y. Wang, Y. Xu, K. Ma, C. An, C. He, Z. Wei, F. Gao and J. Hou, *Adv. Mater.*, 2020, **32**, 1908205.
15. J. Qin, C. An, J. Zhang, K. Ma, Y. Yang, T. Zhang, S. Li, K. Xian, Y. Cui, Y. Tang, W. Ma, H. Yao, S. Zhang, B. Xu, C. He and J. Hou, *Sci. China Mater.*, 2020, **63**, 1142.
16. X. Wang, J. Wang, J. Han, D. Huang, P. Wang, L. Zhou, C. Yang, X. Bao and R. Yang, *Nano Energy*, 2021, **81**, 105612.
17. D. Hu, Q. Yang, H. Chen, F. Wobben, V. M. Le Corre, R. Singh, T. Liu, R. Ma, H. Tang, L. J. A. Koster, T. Duan, H. Yan, Z. Kan, Z. Xiao and S. Lu, *Energy Environ. Sci.*, 2020, **13**, 2134.
18. L. Nian, Y. Kan, K. Gao, M. Zhang, N. Li, G. Zhou, S. B. Jo, X. Shi, F. Lin, Q. Rong, F. Liu, G. Zhou and A. K. Y. Jen, *Joule*, 2020, **4**, 2223.
19. J. Min, Y. N. Luponosov, N. Gasparini, M. Richter, A. V. Bakirov, M. A. Shcherbina, S. N. Chvalun, L. Grodd, S. Grigorian, T. Ameri, S. A. Ponomarenko and C. J. Brabec, *Adv. Energy Mater.*, 2015, **5**, 1500386.
20. H. Tang, H. Chen, C. Yan, J. Huang, P. W. K. Fong, J. Lv, D. Hu, R. Singh, M. Kumar, Z. Xiao, Z. Kan, S. Lu and G. Li, *Adv. Energy Mater.*, 2020, **10**, 2001076.
21. L. Ye, X. Jiao, M. Zhou, S. Zhang, H. Yao, W. Zhao, A. Xia, H. Ade and J. Hou, *Adv. Mater.*, 2015, **27**, 6046.
22. Z. Li, K. Jiang, G. Yang, J. Y. L. Lai, T. Ma, J. Zhao, W. Ma and H. Yan, *Nat. Commun.*, 2016, **7**, 13094.
23. H. Fu, Z. Wang and Y. Sun, *Angew. Chem. Int. Ed.*, 2019, **58**, 4442.
24. C. An, Z. Zheng and J. Hou, *Chem. Commun.*, 2020, **56**, 4750.
25. B. Qiu, Z. Chen, S. Qin, J. Yao, W. Huang, L. Meng, H. Zhu, Y. Yang, Z.-G. Zhang and Y. Li, *Adv. Mater.*, 2020, **32**, 1908373.
26. X. Cheng, M. Li, Z. Guo, J. Yu, G. Lu, L. Bu, L. Ye, H. Ade, Y. Chen and Y. Geng, *J. Mater. Chem. A*, 2019, **7**, 23008.
27. K. Gao, S. B. Jo, X. Shi, L. Nian, M. Zhang, Y. Kan, F. Lin, B. Kan, B. Xu, Q. Rong, L. Shui, F. Liu, X. Peng, G. Zhou, Y. Cao and A. K.-Y. Jen, *Adv. Mater.*, 2019, **31**, 1807842.
28. X. Xue, K. Weng, F. Qi, Y. Zhang, Z. Wang, J. Ali, D. Wei, Y. Sun, F. Liu, M. Wan, J. Liu and L. Huo, *Adv. Energy Mater.*, 2019, **9**, 1802686.
29. X. Bi, Z. Wu, T. Zhang, C. An, Y. Xu, K. Ma, S. Li, S. Zhang, H. Yao, B. Xu, H. Y. Woo, S. Cao and J. Hou, *ACS Appl. Mater. Interfaces*, 2020, **12**, 24184−24191.
30. W. Zhao, S. Li, H. Yao, S. Zhang, Y. Zhang, B. Yang and J. Hou, *J. Am. Chem. Soc.*, 2017, **139**, 7148.
31. K. Sun, Z. Xiao, S. Lu, W. Zajaczkowski, W. Pisula, E. Hanssen, J. M. White, R. M. Williamson, J. Subbiah, J. Ouyang, A. B. Holmes, W. W. H. Wong and D. J. Jones, *Nat. Commun.*, 2015, **6**, 6013.
32. B. Kan, Q. Zhang, F. Liu, X. Wan, Y. Wang, W. Ni, X. Yang, M. Zhang, H. Zhang, T. P. Russell and Y. Chen, *Chem. Mater.*, 2015, **27**, 8414.
33. Y. Guo, M. Li, Y. Zhou, J. Song, Z. Bo and H. Wang, *Macromolecules*, 2017, **50**, 7984.
34. J.-L. Bredas, *Mater. Horiz.*, 2014, **1**, 17.
35. R. F. W. Bader, M. T. Carroll, J. R. Cheeseman and C. Chang, *J. Am. Chem. Soc.*, 1987, **109**, 7968.
36. M. Ans, K. Ayub, I. A. Bhatti and J. Iqbal, *RSC Advances*, 2019, **9**, 3605.
37. N. Gasparini, M. Salvador, S. Strohm, T. Heumueller, I. Levchuk, A. Wadsworth, J. H. Bannock, J. C. de Mello, H.-J. Egelhaaf, D. Baran, I. McCulloch and C. J. Brabec, *Adv. Energy Mater.*, 2017, **7**, 1700770.
38. L. Ke, J. Min, M. Adam, N. Gasparini, Y. Hou, J. D. Perea, W. Chen, H. Zhang, S. Fladischer, A.-C. Sale, E. Spiecker, R. R. Tykwinski, C. J. Brabec and T. Ameri, *Adv. Energy Mater.*, 2016, **6**, 1502355.
39. P. N. Murgatroyd, *J. Phys. D: Appl. Phys.*, 1970, **3**, 151.
40. S. R. Cowan, A. Roy and A. J. Heeger, *Phys. Rev. B*, 2010, **82**, 245207.
41. I. Riedel, J. Parisi, V. Dyakonov, L. Lutsen, D. Vanderzande and J. C. Hummelen, *Adv. Funct. Mater.*, 2004, **14**, 38.
42. K. Vandewal, J. Benduhn and V. C. Nikolis, *Sustain, Energ. Fuels*, 2018, **2**, 538.
43. J. Hou, O. Inganäs, R. H. Friend and F. Gao, *Nat. Mater.*, 2018, **17**, 119.
44. J. Yao, T. Kirchartz, M. S. Vezie, M. A. Faist, W. Gong, Z. He, H. Wu, J. Troughton, T. Watson, D. Bryant and J. Nelson, *Phys. Rev. Appl.*, 2015, **4**, 014020.
45. N. An, Y. Cai, H. Wu, A. Tang, K. Zhang, X. Hao, Z. Ma, Q. Guo, H. S. Ryu, H. Y. Woo, Y. Sun and E. Zhou, *Adv. Mater.*, 2020, **32**, 2002122.
46. Q. Liu, Y. Wang, J. Fang, H. Liu, L. Zhu, X. Guo, M. Gao, Z. Tang, L. Ye, F. Liu, M. Zhang and Y. Li, *Nano Energy*, 2021, **85**, 105963.
47. S. Liu, J. Yuan, W. Deng, M. Luo, Y. Xie, Q. Liang, Y. Zou, Z. He, H. Wu and Y. Cao, *Nat. Photon.*, 2020, **14**, 300.
48. H. Alexander, B. Wim, G. James, S. Eric, G. Eliot, K. Rick, M. Alastair, C. Matthew, R. Bruce and P. Howard, *J. Phys.: Conf. Ser.*, 2010, **247**, 012007.
49. J. H. Carpenter, A. Hunt and H. Ade, *J. Electron Spectrosc. Relat. Phenom.*, 2015, **200**, 2.
50. X. Jiao, L. Ye and H. Ade, *Adv. Energy Mater.*, 2017, **7**, 1700084.
51. E. Gann, A. T. Young, B. A. Collins, H. Yan, J. Nasiatka, H. A. Padmore, H. Ade, A. Hexemer and C. Wang, *Rev. Sci. Instrum.*, 2012, **83**, 045110.